

Article

# Crystal Structures of the 43 kDa ATPase Domain of *Xanthomonas Oryzae* pv. *Oryzae* Topoisomerase IV ParE Subunit and its Complex with Novobiocin

Ha Yun Jung <sup>1</sup> and Yong-Seok Heo <sup>1,\*</sup> 

Department of Chemistry, Konkuk University, 120 Neungdong-ro, Gwangjin-gu, Seoul 05029, Korea; win0531@naver.com

\* Correspondence: ysheo@konkuk.ac.kr

Received: 29 October 2019; Accepted: 4 November 2019; Published: 5 November 2019



**Abstract:** Topoisomerase IV, one of the best-established antibacterial targets, is an enzyme crucial for chromosome segregation and cell division by catalyzing changes in DNA topology through breaking and rejoining DNA. This enzyme functions as a heterotetramer consisting of two ParC and two ParE subunits. Aminocoumarin class inhibitors target the ParE subunit, while widely used quinolones target the ParC subunit. Here, we determined the crystal structure of the ParE 43 kDa ATPase domain from *Xanthomonas oryzae* pv. *oryzae*. Size exclusion chromatography showed that the ParE ATPase domain exists as a monomer in solution, while it dimerizes when ATP is added. Structural comparison with the structure of *Escherichia coli* ParE in complex with an ATP analogue showed large conformational change of the subdomains within the protein. We also determined the structure of the ParE ATPase domain in complex with novobiocin, a natural product aminocoumarin class inhibitor, revealing its binding mode and the structural change within the ATP-binding site induced by novobiocin binding. These results could provide a basis for the design of more potent topoisomerase IV inhibitors with improved antibacterial activity.

**Keywords:** crystal structure; bacterial type II topoisomerase; topoisomerase IV; ParE; novobiocin

## 1. Introduction

Bacterial type II topoisomerases change the topological state of DNA for the initiation of DNA replication and decatenation of daughter chromosomal DNA at the end of replication [1–4]. Bacteria express two highly similar type II topoisomerases, topoisomerase IV and DNA gyrase. These enzymes introduce a transient break into one DNA segment (G segment) and pass another DNA segment (T segment) through the break, which is then resealed [5,6]. Topoisomerase IV is a heterotetramer consisting of two ParC and two ParE subunits. The corresponding DNA gyrase subunits are named GyrA and GyrB [7]. They utilize the energy of ATP hydrolysis for their catalytic activity [8,9]. The transported T-segment DNA is trapped by ATP-dependent dimerization of the ATPase domains of ParE or GyrB before being presented to the cleavage site of the G-segment DNA [10–12]. In topoisomerase IV, the 43 kDa N-terminal domain of ParE is the ATPase domain for the capture of T segment and the C-terminal domain is involved in the interaction with ParC subunit and the G segment [7]. The ParC subunit is composed of the N-terminal domain for the breakage and reunion of the G-segment DNA, the gate for the passing of T segment, and the C-terminal domain for DNA binding [7].

Several sites on bacterial type II topoisomerases have been identified as the targeting sites of natural products and synthetic inhibitors [13–15]. Clinically important fluoroquinolones antibiotics, such as ciprofloxacin, stabilize a covalent ParC/GyrA–DNA complex, thereby interfering with DNA

resealing at the DNA cleavage gate [16]. Aminocoumarin antibiotics, such as novobiocin, target the ATP-binding site of ParE/GyrB [17].

To date, several structures of ParE protein have been reported. The structure of *Escherichia coli* ParE 43 kDa ATPase domain in complex with an ATP analogue showed the dimerization mode of this protein, and its complex structure with novobiocin also revealed the binding mode underlying its antibacterial potency [18]. The crystal structure of ParE from *Francisella tularensis* subsp. *holarctica* elucidated its monomeric state without ATP, while the structure of *Staphylococcus aureus* ParE showed that it can exist as a dimer even in the absence of ATP [19,20]. The structure of *Streptococcus pneumoniae* ParE in complex with ADPNP and a DNA duplex revealed how the T-segment DNA is captured and transported by a type II topoisomerase [21].

*Xanthomonas oryzae* pv. *oryzae* (*Xoo*) is a Gram-negative rod-shaped bacterium that causes bacterial blight rice, which is one of the most problematic diseases in rice-growing countries [22]. Although bacterial blight is the most important rice disease from an economic point of view, there is currently no effective antibacterial agent against *Xoo*. Here, the crystal structure of the 43 kDa ATPase domain of *Xoo* ParE was presented, demonstrating its structural differences from other ParE proteins. We also determined the co-crystal structure of the protein in complex with novobiocin to understand its binding mode and inhibition mechanism. These structures can provide an insight for the mechanism of ParE dimerization and information for discovery of an effective pesticide against bacterial blight.

## 2. Materials and Methods

### 2.1. Cloning and Protein Preparation

The cloning, expression, and purification of the 43 kDa ATPase domain of *Xoo* ParE have been reported earlier [23]. Briefly, the gene encoding the ATPase domain (residues 45–433) of the ParE subunit was amplified from bacterial cells of *X. oryzae* pv. *oryzae* KACC10331 strain and then subcloned into pET-15b vector (Novagen, Madison, WI, USA). The protein was overexpressed with an N-terminal 6His-tag in *E. coli* BL21 (DE3) cells, grown in LB medium, and induced by adding 0.5 mM isopropyl  $\beta$ -D-1-thiogalactopyranoside (IPTG) at 18 °C for 16 h. The cells were disrupted by sonication in lysis buffer (20 mM Tris pH 8.0, 100 mM NaCl and 20 mM imidazole). The supernatant was then loaded onto an Ni-chelated HisTrap FF crude column (GE Healthcare, Chicago, IL, USA), and the bound protein was eluted with elution buffer (20 mM Tris pH 8.0, 100 mM NaCl and 400 mM imidazole). The protein was subsequently loaded onto a HiTrap Q HP column (GE Healthcare, Chicago, IL, USA) and eluted with a linear gradient to a buffer containing 20 mM Tris pH 8.0 and 1.0 M NaCl. The eluted protein was further purified by gel filtration chromatography using a HiTrap 26/60 Sephacryl S-200 HR column (GE Healthcare, Chicago, IL, USA) which had been pre-equilibrated with buffer containing 20 mM Tris pH 8.0 and 100 mM NaCl.

### 2.2. Crystallization, Data Collection, and Structure Determination

Purified protein was concentrated to 25.0 mg/ml by centrifugal ultrafiltration (Amicon) in 20 mM Tris and 100 mM NaCl. Crystals were obtained by the hanging-drop vapor diffusion method at 293 K by mixing 1  $\mu$ L protein solution with 1  $\mu$ L reservoir solution. The reservoir solution for apo-crystal contained 0.1 M Na HEPES pH 7.6, 2% PEG 400 and 1.8 M ammonium sulfate. *Xoo* ParE-novobiocin complex crystals were grown with 0.1 M Na HEPES pH 7.6, 2% PEG 400 and 2.0 M ammonium sulfate after 1 h incubation with 3 mM novobiocin. Both the apo and novobiocin complex crystals appeared in a week. Crystals were cryoprotected by brief immersion in a reservoir solution, supplemented with 20% glycerol, flash frozen in liquid nitrogen. X-ray diffraction data of the apo and complex crystals were collected to 2.20 Å and 2.30 Å resolution, respectively, on beamline 5C at Pohang Light Source (PLS), South Korea. Data were processed with HKL2000 (HKL research Inc., Charlottesville, VA, USA) [24], and an initial molecular replacement (MR) model of the apo structure was obtained using Phase in the CCP4 package with the crystal structure of *E. coli* ParE (PDB code 1s16) as a search

model [25]. Due to the conformational variability of ParE ATPase domain, domain 1 (residues 1 to 217) and domain 2 (residues 218 to 390) were separated when used as search models. The MR solution model was refined with Refmac [26], and manual model building was performed using the COOT program [27]. In both the apo and novobiocin complex structures, several residues in the N-terminal region (residues 45–59), domain 1 region (residues 138–154), and C-terminal region (residues 423–433) were not observed. The data collection and refinement statistics are summarized in Table 1. The coordinate and structure factors for the apo and novobiocin complex have been deposited in Protein Data Bank (<http://www.rcsb.org>) under accession codes 3LNU and 3LPS, respectively.

**Table 1.** Data collection and refinement statistics.

	Apo	Novobiocin Complex
Data Collection		
X-ray source	PLS 5C	PLS 5C
Wavelength (Å)	1.0000	1.0000
Space group	$P4_22_12$	$P4_22_12$
Cell dimensions		
$a, b, c$ (Å)	105.30, 105.30, 133.76	105.12, 105.12, 135.97
$\alpha, \beta, \gamma$ (°)	90, 90, 90	90, 90, 90
Resolution (Å)	2.20 (2.25–2.20) *	2.29 (2.34–2.30)
$R_{\text{sym}}$ (%)	7.8 (42.7)	8.1 (48.6)
$I/\sigma I$	58.1 (2.3)	55.1 (2.3)
Completeness (%)	99.9 (99.0)	97.2 (94.5)
Redundancy	5.9 (2.5)	5.8 (2.6)
Refinement		
Resolution (Å)	2.20	2.30
No. reflections	38,409	34,790
$R_{\text{work}}/R_{\text{free}}$ (%)	23.6/25.7	22.8/25.3
No. atoms		
Protein	2717	2717
Water	194	187
Heterogen	0	44
R.m.s. deviation		
Bond lengths (Å)	0.005	0.007
Bond angles (°)	1.31	1.23
Ramachandran		
Favored (%)	96.76	96.76
Allowed (%)	2.95	2.95
Outlier (%)	0.29	0.29

\* Values in parentheses are for the outer resolution shell.

### 2.3. Analytical Gel Filtration

The purified apo protein was analyzed using a Superdex 200 Increase 10/300 GL column (GE Healthcare Life Sciences, Chicago, IL, USA) in a buffer containing 20 mM Tris pH 8.0 and 100 mM NaCl with or without 1 mM ATP and 5 mM  $\text{MgCl}_2$ . The novobiocin complex was analyzed in a buffer containing 20 mM Tris pH 8.0, 100 mM NaCl, and 100  $\mu\text{M}$  novobiocin after incubation for 1 h.

## 3. Results

### 3.1. Overall Structure of Apo Form

The Apo structure of *Xoo* ParE 43 kD ATPase domain (residues 45–433) was determined and refined to 2.20 Å resolution with  $R/R_{\text{free}} = 0.236/0.257$  (Table 1). As with the structures of ParE from other bacteria, *Xoo* ParE ATPase domain has two distinct domains: Domain 1 (residues 45–261) comprising five  $\alpha$ -helices and an eight-stranded  $\beta$ -sheet, and domain 2 (residues 262–433) comprising a four-stranded  $\beta$ -sheet supported by three  $\alpha$ -helices in its core and a C-terminal  $\alpha$ -helix (Figure 1A).

The asymmetric unit contains one molecule and crystal packing interaction does not reflect any dimeric interface of ParE shown from the structures of other bacterial ParE proteins. Size exclusion chromatography experiment showed that addition of ATP and magnesium ion into the *Xoo* ParE ATPase domain causes a peak shift of the protein, implying that apo *Xoo* ParE exist as a monomer in the absence of ATP and ATP binding would induce any conformational changes within *Xoo* ParE for dimerization (Figure 1B).

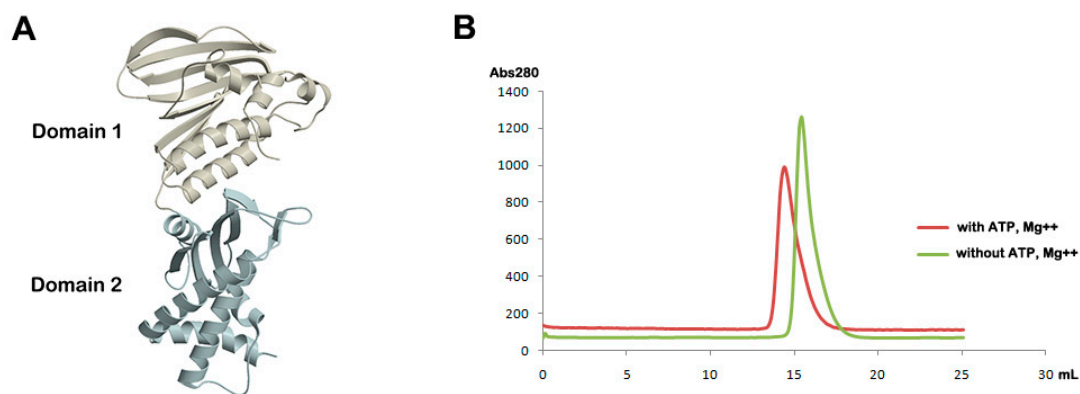


**Figure 1.** Overall structure of *Xoo* ParE. **(A)** The monomeric structure of *Xoo* ParE 43 kD ATPase domain. Domain 1 and domain 2 are shown by different colors. **(B)** Analytical gel-filtration chromatography of *Xoo* ParE in the absence and presence of ATP and magnesium ion.

### 3.2. Structural Comparison of *Xoo* ParE and Other ParE Proteins

In the crystal structure of *E. coli* ParE in complex with ADPNP, the dimer is stabilized by an N-terminal region (residues 1 to 15) that wraps around the other protomer of the dimer through the interaction of the conserved tyrosine residue (Y5 in *E. coli* ParE and Y49 in *Xoo* ParE) with the bound ADPNP [18]. In the apo structure of *Xoo* ParE, the N-terminal region (residues 45 to 59) is not shown due to the absence of an ATP analogue; therefore, it cannot contribute to ParE dimerization. Domain 2 of *E. coli* ParE is also involved in the dimeric interface through the interaction between the C-terminal  $\alpha$ -helices, although the contacts are less extensive. However, domain 2 of *Xoo* ParE displays greater openness than in the *E. coli* ParE (Figure 2A). In the crystal structure of *S. pneumoniae* ParE in complex with ADPNP and a DNA duplex, the dimeric structure of ParE is similar to that of *E. coli* ParE and the DNA duplex penetrates through the hole formed by domain 2 of the dimer, implying ATP binding induces not only dimerization of ParE, but also conformational rearrangement within ParE for the capture of the T-segment DNA (Figure 2B) [21]. Interestingly, the structure of *S. aureus* ParE is a dimeric form even in the absence of ATP or any ATP analogue (Figure 2C) [19]. However, the relative orientation between domain 1 and domain 2 in the structure is markedly different from those of *E. coli* or *S. pneumoniae* ParE in complex with ADPNP, and is rather similar to that of *Xoo* ParE. The exceptionally long C-terminal  $\alpha$ -helix of *S. aureus* ParE may enable the unique dimerization with the greater openness of the T-segment binding hole, suggesting the dimeric form is much less stable than the one with ATP. The apo structure of *F. tularensis* ParE is a monomeric form and similar to *Xoo* ParE structure (Figure 2D) [20]. The lengths of the C-terminal  $\alpha$ -helices of both *F. tularensis* ParE and *Xoo* ParE are probably not enough to induce dimerization in the absence of ATP.

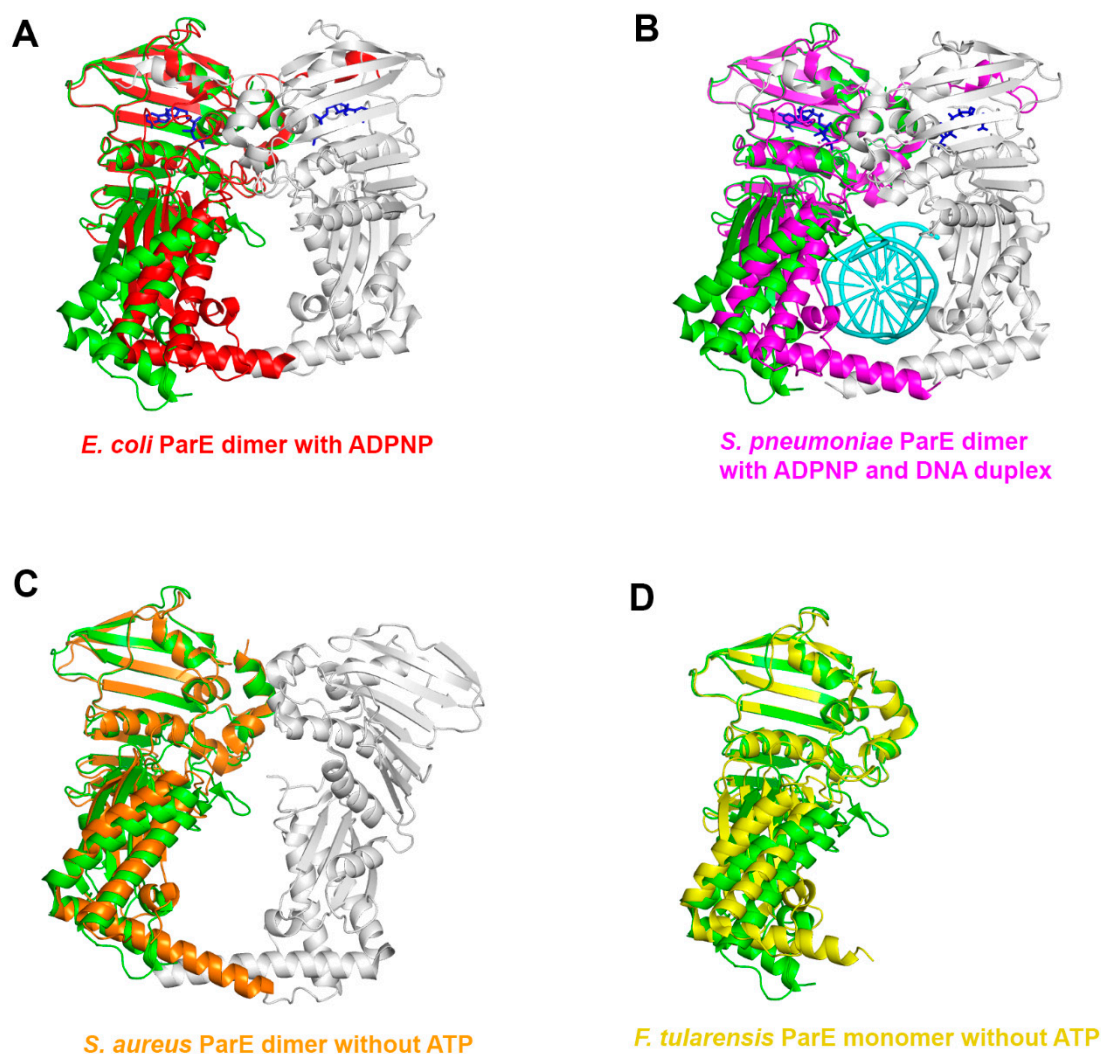


**Figure 2.** Structural comparison of ParE ATPase domains. (A) Comparison of *Xoo* ParE (green) with the dimeric structure of *E. coli* ParE (red and gray, PDB code 1S16) in complex with ADPNP (blue). (B) Comparison of *Xoo* ParE (green) with the dimeric structure of *S. pneumoniae* ParE (purple and gray, PDB code 5J5Q) in complex with ADPNP (blue) and a DNA duplex (cyan). (C) Comparison of *Xoo* ParE (green) with the apo structure of *S. aureus* ParE dimer (orange and gray, PDB code 3URL). (D) Comparison of *Xoo* ParE (green) with the monomeric structure of *F. tularensis* ParE (yellow, PDB code 4HXZ).

### 3.3. Structure of *Xoo* ParE in Complex with Novobiocin

The structure of *Xoo* ParE 43 kD ATPase domain in complex with novobiocin was determined and refined to 2.30 Å resolution with  $R/R_{\text{free}} = 0.228/0.253$  (Table 1). Superimposing ParE in the ParE–novobiocin complex with its apo form yielded an rms deviation of 0.19 Å for all C $\alpha$  atoms and indicated no significant overall structural changes. As expected, size exclusion chromatography showed that the *Xoo* ParE–novobiocin complex behaves like a monomer as the apo form of *Xoo* ParE, implying the binding of novobiocin does not induce any conformational change for dimerization. The novobiocin-binding site is located in domain 1 and can be divided into two distinct sites (Figure 3). The lower binding site partially overlaps with the ATP-binding site, where the noviose moiety of novobiocin occupies the same site occupied by the adenine moiety of ATP. The upper binding site overlaps the binding site of the conserved tyrosine residue within the N-terminal region of the other protomer, occupied by coumarin and the hydroxyl benzoate isoprenyl moiety of novobiocin. In the

dimeric structure of *E. coli* ParE in complex with ADPNP, the conserved tyrosine residue in the N-terminal region interacts with the bound ADPNP of the other protomer through the key hydrogen bond, which contributes to the stabilization of the dimer. These findings suggest that the antibacterial potency of novobiocin is a consequence of not only the direct inhibition of ATP binding, but also the prevention of ParE dimerization, which are essential for the catalytic activity of topoisomerase IV.

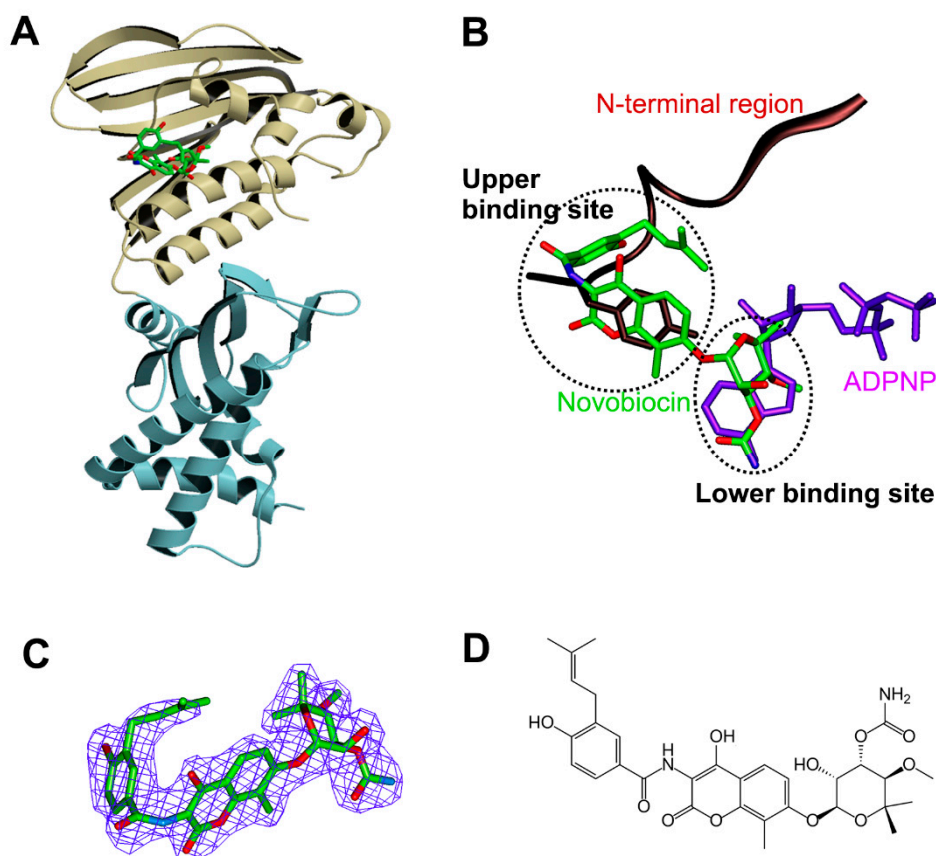


**Figure 3.** Structure of *Xoo* ParE in complex with novobiocin. (A) Overall structure of *Xoo* ParE in complex with novobiocin. Novobiocin (atomic color) is binding to domain 1. (B) Two distinct regions of the novobiocin binding site are indicated as dotted circles. Novobiocin in the complex structure of *Xoo* ParE is overlaid onto the dimeric structure of *E. coli* ParE in complex with ADPNP. The bound ADPNP and N-terminal region including the conserved tyrosine residue are colored purple and brown, respectively. (C)  $2f_o-f_c$  composite omit map ( $1.2\sigma$  contour level) at novobiocin in the complex structure, calculated at 2.30 Å resolution. (D) Chemical structure of novobiocin.

The noviose moiety of novobiocin forms two hydrogen bonds with the side chain of Asp113 and the backbone oxygen atom of Asn86 (Figure 4A). The side chains of Asn86, Met118, and Ile134 also interact with the moiety through VDW contacts. The coumarin ring moiety forms a hydrogen bond with Arg176 and VDW interaction with Pro119. The  $\pi$ - $\pi$  stacking interaction between the coumarin ring and Arg116 would also contribute to the binding energy of the *Xoo* ParE-novobiocin complex. The hydroxyl benzoate isoprenyl moiety forms a hydrogen bond with Asp121 and hydrophobic interaction with Pro119 and Ile134. Although the binding of novobiocin does not change the overall structure of *Xoo* ParE, several residues adapt their side chain conformations for optimal interaction with novobiocin (Figure 4B). Asp121 changes its conformation to make a hydrogen bond with the hydroxyl benzoate group, and Pro119 and Arg116 also change their conformation for more tight contacts with the coumarin moiety of novobiocin.

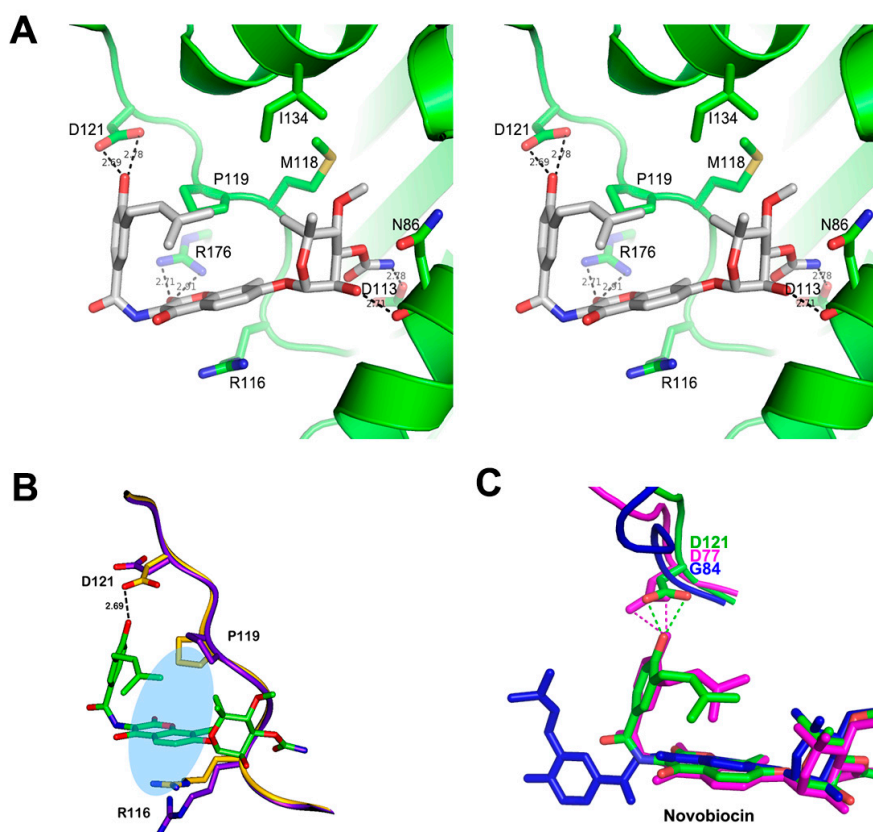


**Figure 4.** Interaction of novobiocin in the complex. (A) Stereoview of the detailed interactions of novobiocin with *Xoo* ParE. The carbon atoms from novobiocin and *Xoo* ParE are colored white and green, respectively. The residues of *Xoo* ParE involved in the interaction are labelled and hydrogen bonds are indicated with dashed lines. (B) Conformational change of the side chains of the residues in the novobiocin-binding site of *Xoo* ParE. The carbon atoms of *Xoo* ParE from the apo form and the novobiocin complex are colored purple and yellow, respectively. The ellipse indicates the interaction of the coumarin moiety of novobiocin with Pro119 and Arg116. (C) Structural comparison of novobiocin in the complex structures. The novobiocin complex structures with *Xoo* ParE (green), *E. coli* ParE (purple, PDB code 1S14), and *S. aureus* ParE (blue, PDB code 4URN) are superimposed.

The binding mode of novobiocin to *Xoo* ParE is very similar to that in the *E. coli* ParE–novobiocin complex, but different from that in the *S. aureus* ParE–novobiocin complex (Figure 4C) [18,19]. The hydroxyl benzoate group folds back onto the coumarin ring in the *Xoo* ParE–novobiocin and *E. coli* ParE–novobiocin complexes, whereas novobiocin in *S. aureus* ParE exhibits an extended conformation. Asp121 of *Xoo* ParE and Asp77 of *E. coli* ParE form hydrogen bonds with the hydroxyl benzoate group of novobiocin. However, the corresponding residue in *S. aureus* ParE is Gly84. Due to the lack of this hydrogen bond in the *S. aureus* ParE–novobiocin complex, the hydroxyl benzoate group could swing out to form the extended conformation.

#### 4. Discussion

Type II topoisomerases mediate the capture of the T-segment DNA and its passage through a transient break of the G-segment DNA using ATP hydrolysis. The mechanism of this molecular machine which arranges these processes, including ATP binding, hydrolysis, breakage and reunion of the G-segment DNA, transport of the T-segment DNA, and product release, is of key importance in understanding the function of type II topoisomerases. Dimerization, mediated by the 43 kDa ATPase domain of ParE in the presence of ATP, was thought to be responsible for the conversion of the open hole into the closed hole that captures the T-segment DNA duplex through conformational changes

within the domain. In the structure of *Xoo* ParE, the monomeric protein exhibited greater openness of domain 2 than other dimeric structures of ParE. As the 43 kDa ATPase domain of ParE is a truncated form without the C-terminal domain which is involved in the interaction with ParC subunit, the extent of openness of domain 2 may be different in full-length ParE proteins.

Aminocoumarin antibiotics including novobiocin were unsuccessful in the clinic. The oral form of novobiocin has been withdrawn from the market due to lack of efficacy. However, the application of aminocoumarins as pesticides against *Xanthomonas oryzae* pv. *oryzae* can be helpful to overcome bacterial blight in rice. The binding mode of novobiocin to *Xoo* ParE was different from that of *S. aureus* ParE due to the amino acid difference of the binding site. This difference of the binding mode can result in different potency of novobiocin to other bacteria. The enzyme assays for the inhibition of ATPase activities of topoisomerase IV of *E. coli* and *S. aureus* by novobiocin have shown the  $K_i$  values of 0.160  $\mu$ M and 0.900  $\mu$ M, respectively, implying the compound is more potent in *E. coli* than *S. aureus* [28,29]. The structure of the *Xoo* ParE-novobiocin complex presented here reveals the binding mode of novobiocin and, thus, can assist in the prospective design of novel inhibitors of *Xoo* ParE with improved safety and efficacy in future.

**Author Contributions:** Conceptualization, H.Y.J. and Y.-S.H.; methodology, H.Y.J.; validation, H.Y.J. and Y.-S.H.; formal analysis, H.Y.J. and Y.-S.H.; investigation, Y.-S.H.; writing—original draft preparation, H.Y.J. and Y.-S.H.; visualization, H.Y.J. and Y.-S.H.; supervision, Y.-S.H.; project administration, Y.-S.H.; funding acquisition, Y.-S.H.

**Funding:** This research was supported by the Basic Science Research Program of the National Research Foundation of Korea (NRF) funded by the Ministry of Science and ICT (NRF-2018R1A2B6009372).

**Acknowledgments:** We are grateful to the staff of Beamline 5C at the Pohang Accelerator Laboratory (PAL), Korea.

**Conflicts of Interest:** The authors declare no conflict of interest. The funders had no role in the design of the study; in the collection, analyses, or interpretation of data; in the writing of the manuscript, or in the decision to publish the results.

## References

1. Pommier, Y.; Sun, Y.; Huang, S.N.; Nitiss, J.L. Roles of eukaryotic DNA topoisomerases in transcription, replication and genome stability. *Nat. Rev. Mol. Cell Biol.* **2016**, *17*, 703–721. [[CrossRef](#)] [[PubMed](#)]
2. Nitiss, J.L. DNA topoisomerase II and its growing repertoire of biological functions. *Nat. Rev. Cancer* **2009**, *9*, 327–337. [[CrossRef](#)] [[PubMed](#)]
3. Schoeffler, A.J.; Berger, J.M. DNA topoisomerases: Harnessing and constraining energy to govern chromosome topology. *Q. Rev. Biophys.* **2008**, *41*, 41–101. [[CrossRef](#)] [[PubMed](#)]
4. Vos, S.M.; Tretter, E.M.; Schmidt, B.H.; Berger, J.M. All tangled up: How cells direct, manage and exploit topoisomerase function. *Nat. Rev. Mol. Cell Biol.* **2011**, *12*, 827–841. [[CrossRef](#)] [[PubMed](#)]
5. Mizuuchi, K.; Fisher, L.M.; O’Dea, M.H.; Gellert, M. DNA gyrase action involves the introduction of transient double-strand breaks into DNA. *Proc. Natl. Acad. Sci. USA* **1980**, *77*, 1847–1851. [[CrossRef](#)] [[PubMed](#)]
6. Corbett, K.D.; Schoeffler, A.J.; Thomsen, N.D.; Berger, J.M. The structural basis of substrate specificity in DNA topoisomerase IV. *J. Mol. Biol.* **2005**, *351*, 545–561. [[CrossRef](#)] [[PubMed](#)]
7. Corbett, K.D.; Berger, J.M. Structure, molecular mechanisms, and evolutionary relationships in DNA topoisomerases. *Ann. Rev. Biophys. Biomol. Struct.* **2004**, *33*, 95–118. [[CrossRef](#)]
8. Crisona, N.J.; Strick, T.R.; Bensimon, D.; Croquette, V.; Cozzarelli, N.R. Preferential relaxation of positively supercoiled DNA by *E. coli* topoisomerase IV in single-molecule and ensemble measurements. *Genes Dev.* **2000**, *14*, 2881–2892. [[CrossRef](#)]
9. Ullsperger, C.; Cozzarelli, N.R. Contrasting enzymatic activities of topoisomerase IV and DNA gyrase from *Escherichia coli*. *J. Biol. Chem.* **1996**, *271*, 31549–31555. [[CrossRef](#)]
10. Dekker, N.H.; Rybenkov, V.V.; Duguet, M.; Crisona, N.J.; Cozzarelli, N.R.; Bensimon, D.; Croquette, V. The mechanism of type IA topoisomerases. *Proc. Natl. Acad. Sci. USA* **2002**, *99*, 12126–12131. [[CrossRef](#)]
11. Roca, J.; Berger, J.M.; Harrison, S.C.; Wang, J.C. DNA transport by a type II topoisomerase: Direct evidence for a two-gate mechanism. *Proc. Natl. Acad. Sci. USA* **1996**, *93*, 4057–4062. [[CrossRef](#)] [[PubMed](#)]
12. Roca, J. The path of the DNA along the dimer interface of topoisomerase II. *J. Biol. Chem.* **2004**, *279*, 25783–25788. [[CrossRef](#)] [[PubMed](#)]

13. Drlica, K.; Hiasa, H.; Kerns, R.; Malik, M.; Mustaev, A.; Zhao, X. Quinolones: Action and resistance updated. *Curr. Top. Med. Chem.* **2009**, *9*, 981–998. [[CrossRef](#)] [[PubMed](#)]
14. Bax, B.D.; Chan, P.F.; Eggleston, D.S.; Fosberry, A.; Gentry, D.R.; Gorrec, F.; Giordano, I.; Hann, M.M.; Hennessy, A.; Hibbs, M.; et al. Type IIA topoisomerase inhibition by a new class of antibacterial agent. *Nature* **2010**, *466*, 935–940. [[CrossRef](#)] [[PubMed](#)]
15. Chan, P.F.; Srikannathasan, V.; Huang, J.; Cui, H.; Fosberry, A.P.; Gu, M.; Hann, M.M.; Hibbs, M.; Homes, P.; Ingraham, K.; et al. Structural basis of DNA gyrase inhibition by antibacterial QPT-1, anticancer drug etoposide, and moxifloxacin. *Nat. Commun.* **2015**, *6*, 10048. [[CrossRef](#)] [[PubMed](#)]
16. Laponogov, I.; Sohi, M.K.; Veselkov, D.A.; Pan, X.S.; Sawhney, R.; Thompson, A.W.; McAuley, K.E.; Fisher, L.M.; Sanderson, M.R. Structural insight into the quinolone-DNA cleavage complex of type IIA topoisomerases. *Nat. Struct. Mol. Biol.* **2009**, *16*, 667–669. [[CrossRef](#)]
17. Ali, J.A.; Jackson, A.P.; Howells, A.J.; Maxwell, A. The 43-kilodalton N-terminal fragment of the DNA gyrase B protein hydrolyses ATP and binds coumarin drugs. *Biochemistry* **1993**, *32*, 2717–2724. [[CrossRef](#)]
18. Bellon, S.; Parsons, J.D.; Wei, Y.; Hayakawa, K.; Swenson, L.L.; Charifson, P.S.; Lippke, J.A.; Aldape, R.; Gross, C.H. Crystal structures of Escherichia coli topoisomerase IV ParE subunit (24 and 43 kilodaltons): A single residue dictates differences in novobiocin potency against topoisomerase IV and DNA gyrase. *Antimicrob. Agents Chemother.* **2004**, *48*, 1856–1864. [[CrossRef](#)]
19. Lu, J.; Patel, S.; Sharma, N.; Soisson, S.M.; Kishii, R.; Takei, M.; Fukuda, Y.; Lumb, K.J.; Singh, S.B. Structures of Kibdelomycin Bound to Staphylococcus Aureus GyrB and Pare Showed a Novel U-Shaped Binding Mode. *ACS Chem. Biol.* **2014**, *9*, 2023–2031. [[CrossRef](#)]
20. Tari, L.W.; Trzoss, M.; Bensen, D.C.; Li, X.; Chen, Z.; Lam, T.; Zhang, J.; Creighton, C.J.; Cunningham, M.L.; Kwan, B.; et al. Pyrrolopyrimidine inhibitors of DNA gyrase B (GyrB) and topoisomerase IV (ParE). Part I: Structure guided discovery and optimization of dual targeting agents with potent, broad-spectrum enzymatic activity. *Bioorg. Med. Chem. Lett.* **2013**, *23*, 1529–1536. [[CrossRef](#)]
21. Laponogov, I.; Pan, X.S.; Veselkov, D.A.; Skamrova, G.B.; Umrekar, T.R.; Fisher, L.M.; Sanderson, M.R. Trapping of the transport-segment DNA by the ATPase domains of a type II topoisomerase. *Nat. Commun.* **2018**, *9*, 2579. [[CrossRef](#)] [[PubMed](#)]
22. Verdier, V.; Vera Cruz, C.; Leach, J.E. Controlling rice bacterial blight in Africa: Needs and prospects. *J. Biotechnol.* **2012**, *159*, 320–328. [[CrossRef](#)] [[PubMed](#)]
23. Shin, H.J.; Yun, M.; Song, J.Y.; Kim, H.J.; Heo, Y.S. Crystallization and X-ray diffraction data collection of topoisomerase IV ParE subunit from Xanthomonas oryzae pv. oryzae. *Acta Crystallogr. Sect. F Struct. Biol. Cryst. Commun.* **2009**, *65*, 612–614. [[CrossRef](#)] [[PubMed](#)]
24. Otwinowski, Z.; Minor, W. Processing of X-ray diffraction data collected in oscillation mode. *Methods Enzymol.* **1997**, *276*, 307–326. [[PubMed](#)]
25. McCoy, A.J.; Grosse-Kunstleve, R.W.; Adams, P.D.; Winn, M.D.; Storoni, L.C.; Read, R.J. Phaser crystallographic software. *J. Appl. Crystallogr.* **2007**, *40*, 658–674. [[CrossRef](#)]
26. Murshudov, G.N.; Vagin, A.A.; Dodson, E.J. Refinement of macromolecular structures by the maximum-likelihood method. *Acta Crystallogr. D Biol. Crystallogr.* **1997**, *53*, 240–255. [[CrossRef](#)]
27. Emsley, P.; Lohkamp, B.; Scott, W.G.; Cowtan, K. Features and development of Coot. *Acta Crystallogr. Sect. D Biol. Crystallogr.* **2010**, *66*, 486–501. [[CrossRef](#)]
28. Mani, N.; Gross, C.H.; Parsons, J.D.; Hanzelka, B.; Muh, U.; Mullin, S.; Liao, Y.; Grillot, A.L.; Stamos, D.; Charifson, P.S.; et al. In vitro characterization of the antibacterial spectrum of novel bacterial type II topoisomerase inhibitors of the aminobenzimidazole class. *Antimicrob. Agents Chemother.* **2006**, *50*, 1228–1237. [[CrossRef](#)]
29. Charifson, P.S.; Grillot, A.L.; Grossman, T.H.; Parsons, J.D.; Badia, M.; Bellon, S.; Deininger, D.D.; Drumm, J.E.; Gross, C.H.; LeTiran, A.; et al. Novel dual-targeting benzimidazole urea inhibitors of DNA gyrase and topoisomerase IV possessing potent antibacterial activity: Intelligent design and evolution through the judicious use of structure-guided design and structure-activity relationships. *J. Med. Chem.* **2008**, *51*, 5243–5263. [[CrossRef](#)]

